Hindawi
Geofluids
Volume 2021, Article ID 6020850, 17 pages
https://doi.org/10.1155/2021/6020850

Research Article

Thermal Maturation Regime Revisited in the Dongying Depression, Bohai Bay Basin, East China

Haiping Huang,[1,2,3] **Hong Zhang**,[1] **Zheng Li**,[4] **and Mei Liu**[2]

[1]*School of Geosciences, Yangtze University, Wuhan, 430100 Hubei, China*
[2]*School of Energy Resource, China University of Geosciences (Beijing), Beijing 100083, China*
[3]*Department of Geoscience, University of Calgary, Calgary, Alberta, Canada T2N 1N4*
[4]*Geology Scientific Research Institute of Shengli Oilfield Company, Sinopec, Dongying 257015, China*

Correspondence should be addressed to Haiping Huang; huah@ucalgary.ca

Received 20 July 2021; Accepted 7 September 2021; Published 24 September 2021

Academic Editor: Lanxiao Hu

To the accurate reconstruction of the hydrocarbon generation history in the Dongying Depression, Bohai Bay Basin, East China, core samples of the Eocene Shahejie Formation from 3 shale oil boreholes were analyzed using organic petrology and organic geochemistry methods. The shales are enriched in organic matter with good to excellent hydrocarbon generation potential. The maturity indicated by measured vitrinite reflectance (%R_o) falls in the range of 0.5–0.9% and increases with burial depth in each well. Changes in biomarker and aromatic hydrocarbon isomer distributions and biomarker concentrations are also unequivocally correlated with the thermal maturity of the source rocks. Maturity/depth relationships for hopanes, steranes, and aromatic hydrocarbons, constructed from core data indicate different well locations, have different thermal regimes. A systematic variability of maturity with geographical position along the depression has been illustrated, which is a dependence on the distance to the Tanlu Fault. Higher thermal gradient at the southern side of the Dongying Depression results in the same maturity level at shallower depth compared to the northern side. The significant regional thermal regime change from south to north in the Dongying Depression may exert an important impact on the timing of hydrocarbon maturation and expulsion at different locations. Different exploration strategies should be employed accordingly.

1. Introduction

Determining the thermal maturity of source rocks is crucial for the prediction of petroleum generation time and the exploration potential in a sedimentary basin. Various petrological and geochemical methods can be applied for thermal history reconstruction, which include vitrinite reflectance (%R_o), Rock-Eval, T_{max}, kerogen H/C ratio, degree of biomarker isomerization, homogenization temperature in fluid inclusions, apatite fission track analysis, and many other maturity indicators [1–5]. Widely applied petroleum system modeling techniques largely rely on the reaction kinetics of kerogens and thermal maturity of source rocks to predict the timing of oil and gas generation and identify hydrocarbon production targets [6–8]. Vitrinite reflectance is considered the most suitable and widely used tool for such purposes as it can be universally applied in strata deposited after the late Devonian [9]. Oil and gas generation stages are usually classified on the basis of %R_o values even though the kinetics of kerogen thermal cracking differs from vitrinite particle rearrangement [6–8]. T_{max} of the Rock-Eval pyrolysis offers the easiest way to assess source rock maturity levels [10]; however, T_{max} suppression may occur in some liptinite enriched kerogens [11, 12].

The molecular markers present in the extractable organic matter (EOM) reflect different aspects of source rock thermal evolution during diagenetic and catagenetic processes. The relative abundance of thermally unstable biological isomers to the thermally stable geological isomers can indicate the thermal maturity levels of organic matter. There are numerous maturity parameters available in the literature, which have been applied for thermal history reconstruction

and maturity level assessment [2, 13–15]. However, the reaction mechanisms of molecular parameters are much more complex than this generally assumed and no universally valid maturity scale that is available [2]. Most molecular ratios are governed by the rates of generation and/or destruction of isomers of kerogen during catagenesis rather than pure isomerization [16, 17]. Meanwhile, the molecular ratios are highly susceptible to variations in organofacies, kerogen type, and migration effects [18–20]. Caution should be taken when molecular ratios are used in maturity level assessment. van Graas suggested that absolute concentrations of molecular components especially biomarkers rather than isomer ratios are more reliable to indicate the maturity level in the oil generation window (0.6–1.0% Ro) [21]. Nevertheless, to integrate molecular compositions with petrological information is the only way to make the most reasonable interpretation possible [15].

Dongyong Depression, situated at south of the Bohai Bay Basin in eastern China, is a prolific region for oil and gas production. A substantial amount of data becomes available regarding the tectonic framework and structural evolution, depositional systems and stratigraphic records, oil and gas generation potential, and oil family classification [22–26]. Surprisingly, the basic petroleum geological issues such as oil generation threshold depth and thermal maturity scheme of the depression have rarely been acquiescent. Very different oil generation threshold depths have been recognized in the Dongying Depression. Some studies regarded 2,000 m as the top of oil generation window [27–30], while other studies settled the oil generation threshold depth at 2,500 m [31–33] or 3,000 m [34]. The discrepancy in the threshold depth not only results in very different petroleum generations and accumulation times but also substantially different exploration perspectives. Variable vitrinite reflectance measurements from different locations and lithologies might cause such discrepancy, but intrinsic constraints such as variable heat flow may play a more important role. However, no systematic investigation has not been performed. This paper integrates vitrinite reflectance measurement with molecular composition in 3 shale oil exploration wells (FY1, NY1, and LY1) drilled in the Dongying Depression to evaluate the regional thermal maturity variation within stratigraphic units. Systematic differences observed from molecular compositions and vitrinite reflectance measurements at different locations might be rooted from thermal regime variation throughout the depression. The main objectives of the study by characterizing the thermal evolution of organic matter to assess the thermal regime of the Dongying Depression in explaining variable oil generation threshold depths. The integration of two thermal maturity indicator types leads to a better definition of the petroleum system.

2. Geological Background

Dongying Depression with an area of roughly 5,700 km^2 is a typical asymmetric half graben in the Bohai Bay Basin, East China. It is bounded by the Chenjiazhuang High to the north, the Qingtuozi High to the east, the Qingcheng and Binxian highs to the west, and the Luxi Uplift to the south. The depression can be subdivided into four sags (Boxing, Niuzhuang, Lijin, and Minfeng) by several normal faults, one uplift (Central Anticlinal Belt), southern gentle slope, and northern steep slope (Figure 1(a)). Sedimentary sequence filled in the depression is mainly developed in the Cenozoic age as a result of a dextral movement along the Tanlu Fault. Tectonic evolution of the depression can be divided into three stages: (1) the prerift stage of the Mesozoic to Paleozoic basement, (2) the rift stage of the Paleogene fluvial lacustrine sediments, and (3) depression stage of the Neogene fluvial sediments [22]. The thickness of the Cenozoic lacustrine deposits exceeds 5,000 m in some subsiding centers. It consists of the Kongdian, Shahejie, Dongying, Guantao, Minghuazhen, and Pingyuan formations (Figure 1(b)). The Shahejie Formation (Es) contains the main source rocks and sandstone reservoirs in the whole basin and can be further divided into four members, Es1, Es2, Es3, and Es4 (from top to bottom). The Es4 member was developed in saline to hypersaline lacustrine environment. The lower part of the Es4 member consists of mudstones, siltstones, and fine sandstones interbedded with gypsum and halite, while the upper part of the Es4 member consists of grey to black shale, calcareous shale, and mudstone, dolomite as well as marlstone. The Es3 member was formed in a brackish to freshwater lacustrine environment, which is mainly composed of deep lacustrine dark mudstones and calcareous shales. Both members contain important source rocks within the depression, which are dominated by type I-II kerogens with TOC contents up to 18.6% [24, 27, 34]. The reservoirs occur in variable stratigraphic units, which are controlled by faults connected to the source rocks [31, 32].

3. Samples and Methods

Twenty-seven core samples from three shale oil exploration wells in the Dongying Depression were collected in the present study. Fourteen samples were from the Es3 member, and thirteen samples were from the Es4 member. The analytical methods are the same as our previous studies [35, 36]. Briefly, standard Rock-Eval pyrolysis was performed on Rock-Eval VI apparatus with a flame ionization detector [37]. The vitrinite reflectance measurement was carried out in Shengli Oilfield Company by using the MSP-400 microscopic fluorescence spectrometer with a temperature of 22°C and a relative humidity of 20%. Minimum 50 points were measured, and an averaged value was recorded.

The extractable organic matter (EOM) was obtained using Soxhlet extraction for 72 h with dichloromethane (DCM) and methanol (93 : 7 v/v). The EOM was weighed using an inhouse method. About 50 mg of EOM was transferred to a vial and a suite of internal standards (cholestane-d4, adamantane-d16, phenyldodacane-d30, naphthalene-d8, phenanthrene-d10 and 1,1-binaphthalene) that were added, and then the sample was separated into the saturated and aromatic hydrocarbon fractions.

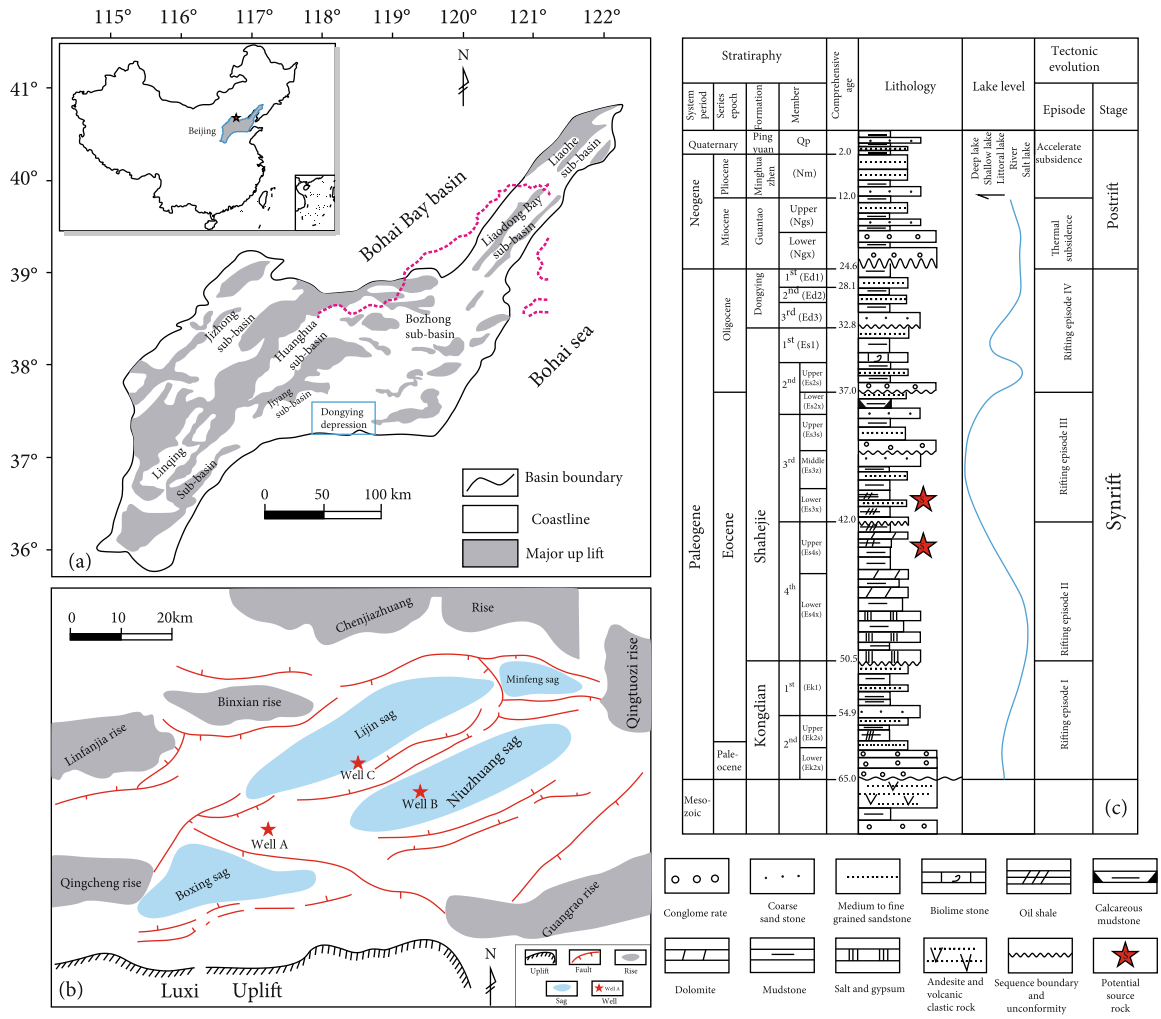

FIGURE 1: Location map of the study area. (a) Schematic map of the Bohai Bay Basin and its location in China. (b) Tectonic setting map of the Dongying Depression showing the uplift, sags, main faults, and shale oil well locations where the samples were obtained. (c) General stratigraphy column of the Dongying Depression (after Zhang et al. [35]).

The saturated and aromatic hydrocarbon fractions were analyzed using GC–MS in both selected ion monitoring and full scan mode (SIM/SCAN) on an Agilent 7890B gas chromatograph linked to an Agilent 5977A MSD system. The DB–1MS fused silica capillary column (60 m × 0.32 mm i.d. × 0.25 μm film thickness) was used for separation. The GC oven temperature for the saturated hydrocarbon fraction was programmed from 50 °C (1 min) to 120 °C at 20 °C/min, then increased to 310 °C at 3 °C/min, which was held for 25 min. The GC oven temperature for the aromatic hydrocarbon fraction was set at 40 °C initially for 5 min, programmed to 325 °C at 4 °C/min, and lasted for 20 min. Helium was used as the carrier gas, and a constant flow rate of 1 ml/min was applied. The temperature of the injector and interface was set at 300 °C. The ion source was operated in the electron ionization (EI) mode at 70 eV. Peak identification and quantitation were performed by comparison of MS standard library in this system and the aforementioned internal standards with known quantities, respectively. No response factor calibration has been performed.

4. Results

4.1. Bulk Geochemistry of Source Rocks. Basic geochemical data of the studied source rocks are listed in Table 1. Pyrolysis results indicate that the Shahejie Formation has excellent organic matter quality, quantity, and hydrocarbon generation potential. The total organic carbon (TOC) contents vary in the range of 1.44–7.66 wt% with an average value of 3.62 wt%, indicating high petroleum generation potential. S1 and S2 values that range from 2.1 to 14.6 mg HC/g rock and 5.0 to 48.3 mg HC/g rock, respectively, are recorded in this formation, with S3 documented to be from 0.1 to 1.1 mg HC/g rock. The calculated hydrogen indices (HI = S2/TOC × 100) for the studied samples vary in the range of 266–630 mg HC/g TOC, with an average of 415, 491 and 338 mg HC/g TOC in wells FY1, NY1, and LY1, respectively. The oxygen indices (OI = S3/TOC × 100) vary in the range of 2–35 mg CO_2/g TOC, with an average of 13 mg CO_2/g TOC. While the HI is fluctuated in each well, it decreases with increasing burial depth due to hydrocarbon

Table 1: Results of Rock-Eval analysis and vitrinite reflectance measurement of studied samples from the Dongying Depression.

Well	Age	Depth (m)	R_o (%)	TOC (%)	S1 (mg/g rock)	S2 (mg/g rock)	S3 (mg/g rock)	T_{max} (°C)	HI (mg/gTOC)	OI (mg/gTOC)	PI
FY1	Es3	3031.5	0.51	1.89	2.09	7.09	0.16	439	375	8	0.23
FY1	Es3	3059.92	0.48	3.4	4.43	16.36	0.26	443	481	8	0.21
FY1	Es3	3125.65	0.54	1.98	2.88	8.86	0.25	445	447	13	0.25
FY1	Es3	3170.14	0.58	7.22	4.58	35.55	0.31	447	492	4	0.11
FY1	Es3	3233.29	0.65	2.17	2.68	7.58	0.23	445	349	11	0.26
FY1	Es4	3316.23	0.76	1.44	2.67	4.97	0.2	433	345	14	0.35
NY1	Es3	3304.1	0.44	2.81	2.49	16.51	0.52	440	588	19	0.13
NY1	Es4	3333.04	0.47	2.5	3.4	12.85	0.56	439	514	22	0.21
NY1	Es4	3372.9	0.53	1.99	3.19	9.98	0.56	443	502	28	0.24
NY1	Es4	3377.84		2.59	3.12	11.46	0.27	445	442	10	0.21
NY1	Es4	3402.73	0.57	7.66	8.69	48.27	0.47	446	630	6	0.15
NY1	Es4	3462.58	0.67	1.88	3.44	5.09	0.66	430	271	35	0.40
LY1	Es3	3582.14	0.51	3.36	6.26	12.54	0.18	443	373	5	0.33
LY1	Es3	3586.16	0.52	3.79	6.93	13.53	0.19	439	357	5	0.34
LY1	Es3	3593.01	0.53	4.51	7.46	17.61	0.09	445	390	2	0.30
LY1	Es3	3598.15	0.53	4.77	8.18	18.08	0.19	443	379	4	0.31
LY1	Es3	3601.21		4.82	9.65	18.73	0.34	442	389	7	0.34
LY1	Es3	3658.46	0.6	5.63	14.64	20.74	0.6	442	368	11	0.41
LY1	Es3	3672.38	0.62	3.27	8.47	11.65	0.41	433	356	13	0.42
LY1	Es3	3674.34	0.62	4.54	8.83	17.88	0.45	442	394	10	0.33
LY1	Es4	3751.14	0.73	3.08	4.93	9.88	0.59	431	321	19	0.33
LY1	Es4	3768.15	0.76	5.05	10.41	13.52	1.13	431	268	22	0.44
LY1	Es4	3771.81	0.76	2.77	4.77	9.37	0.45	434	338	16	0.34
LY1	Es4	3786.16	0.78	2.97	7.14	8.38	0.46	442	282	15	0.46
LY1	Es4	3803.65		4.49	13.25	13.44	0.52	436	299	12	0.50
LY1	Es4	3815.76	0.83	3.63	5.88	9.66	0.61	429	266	17	0.38
LY1	Es4	3830.45	0.86	3.57	5.68	10.36	0.57	441	290	16	0.35

R_o: measured vitrinite reflectance; TOC: total organic carbon; S1: the amount of free hydrocarbons released before 300°C; S2: the amount of hydrocarbons generated from kerogen cracking between 300 to 650°C; S3: the amount of CO2 detected at 390°C; T_{max}: the temperature at which the maximum amount of hydrocarbon is generated from the sample; HI: hydrogen index (= S2/TOC × 100); OI: oxygen index (= S3/TOC × 100); PI: production index [= S1/(S1 + S2)].

generation and expulsion. Cross correlation between HI and OI suggests that the organic matter of the Shahejie Formation comprises primarily of oil-prone kerogen type I-II at the immature stage.

Thermal maturity is an important characteristic that has to be analyzed in a source rock, and it is usually determined by using R_o, T_{max}, and production index [PI = S1/(S1 + S2)]. The vitrinite reflectance values of the studied sample intervals from FY1 range from 0.48% to 0.74%, these in well NY1 from 0.44% to 0.67%, and these in well LY1 from 0.51% to 0.86% (Figure 2(a)). A gradual increase trend with increasing depth of burial can be clearly observed in each well. All source rocks are in early mature to mature conditions with respect to hydrocarbon generation. However, the threshold depth of oil generation (assumed as $R_o = 0.5$ %) in well LY1 is about 500 m deeper than that in well FY1. T_{max} (temperature corresponding to the S2 peak maximum of Rock-Eval pyrolysis) values of the Es3 samples in FY1 range from 439 °C to 447 °C, while one Es4 sample has a lower T_{max} value of 433 °C. T_{max} values of one Es3 sample and four Es4 samples in the shallower part of NY1 increase from 439 °C to 446 °C, but the one deeper Es4 samples have much lower T_{max} value of 430 °C. T_{max} values in LY1 vary from 429 °C to 445 °C without a depth-related trend (Figure 2(b)). The T_{max} values of > 430 °C in source rocks from both Es3 and Es4 suggest that they are thermally mature; however, the correlation between T_{max} and burial depth is poor, likely caused by facies variation or immigrated hydrocarbons [38, 39].

The PI is defined as the free hydrocarbons measured relative to the total hydrocarbon generated during pyrolysis. PI values in wells FY1, NY1, and LY1 vary in the range of 0.11–0.35, 0.13–0.40, and 0.33–0.50, respectively (Table 1), suggesting that the maturities of these source rock intervals are in the early oil window or greater. A general increase trend of the PI values with increasing depth suggests that the burial of organic matter plays the dominant role in hydrocarbon generation (Figure 2(c)). Interestingly, PI

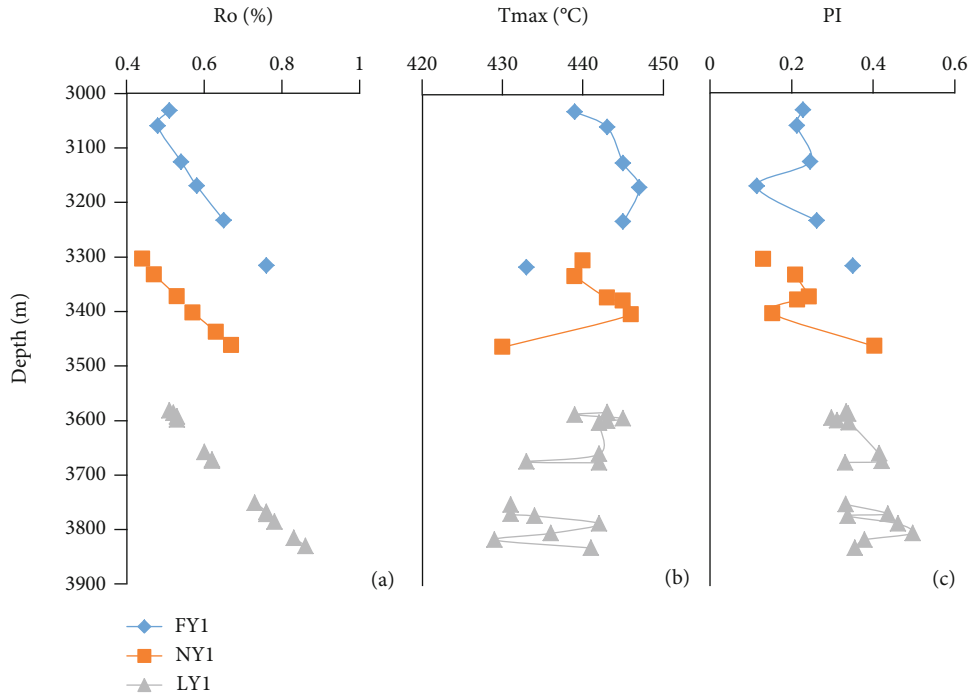

Figure 2: Depth profile of maturity indicators at wells FY1, NY1, and LY1 in the Dongying Depression. (a) Measured vitrinite reflectance. (b) Rock-Eval T_{max}. (c) Production index.

values show a weak inverse correlation to T_{max}, further verifying that T_{max} value is a poor maturity indicator in the current study case.

4.2. Maturity Indicators Derived from Saturated Hydrocarbons. Partial mass chromatograms at m/z 191 display the distribution of tri- and pentacyclic terpanes from wells FY1 and LY1 (Figure 3). Samples shallower than 3200 m in well FY1 and the top sample in well LY1 at 3582 m show very similar distribution patterns, which consist primarily of the ubiquitous hopane series, with the C_{30} 17α, 21β(H)-hopane (C_{30}H) predominating. Tricyclic terpanes (TT) from C_{19} to C_{30} and C_{24} tetracyclic terpane show trace amount compared to the pentacyclic terpanes (PT). With increasing burial depth, the dominance of pentacyclic terpanes is diminished, while the relative proportion of tricyclic terpanes increases consequently. Changes in the pentacyclic terpane region are characterized by the depletion of C_{29}–C_{35} regular hopanes and relative enrichment of rearranged hopanes. The relative abundance of 18α(H)-22,29,30-trisnorneohopane (Ts) increases continuously with burial depth and becomes the dominant peak of the m/z 191 mass chromatogram in the deepest section of LY1. The 18α(H)-30-norneohopane (C_{29}Ts) and C_{30}-diahopane (15α-methyl-17α(H)-27-norhopane, C_{30}D) have also been relatively concentrated (Figure 3).

Classical biomarker maturity parameters measured from GC-MS analyses are listed in Table 2. Isomerization ratios of C_{31}-homohopane 22S/(22S + 22R) have approached the equilibrium values (0.57–0.60) and are no longer sensitive to maturity variation (Table 2). However, it indicates that all samples are at least in the oil generation window since this parameter reaches its equilibrium value prior to the main hydrocarbon generation threshold [2]. The ratio of C_{30} 17β,21α(H)-hopane (moretane, C_{30}M) to C_{30}H decreases with increasing thermal maturity from values of about 0.8 for immature bitumen to values less than 0.15 for mature samples [2]. Samples in the present study have their C_{30}M/C_{30}H ratio < 0.15, suggesting that all samples are mature (Table 2). Again, this ratio has also reached its equilibrium value and cannot be used to differentiate the maturity differences for the studied samples.

The relative abundance of Ts and 17α(H)-22,29,30-trisnorhopane (Tm) has been widely employed as a maturity parameter in a similar organofacies system [2, 15]. The Ts/(Ts + Tm) ratios vary in the range of 0.51–0.86 in FY1, 0.43–0.75 in well NY1, and 0.75–0.95 in well NY1, respectively, showing an increasing trend with increasing burial depth in each well (Figure 4(a)). Evolution profiles of the Ts/(Ts + Tm) ratio in the studied wells suggest a relative consecutive maturity regime at each well location. Ts/(Ts + Tm) ratio values in LY1 approach the maximum value of 1.0, indicating a highly mature status due to deep burial. However, the ratio values in well NY1 are slightly lower than these in well FY1, which is about 300 m shallower at the same ratio value.

C_{30}-diahopane is characterized by high thermal stability, which is even more stable than that of the 18α-neohopane series [40]. Ratios of C_{30}-diahopane to C_{30} hopane [C_{30}D/(C_{30}D + C_{30}H)] increase steadily from 0.05 at the top sample to 0.18 at the bottom in the samples of FY1, and the ratio values increase from 0.15 to 0.63 with

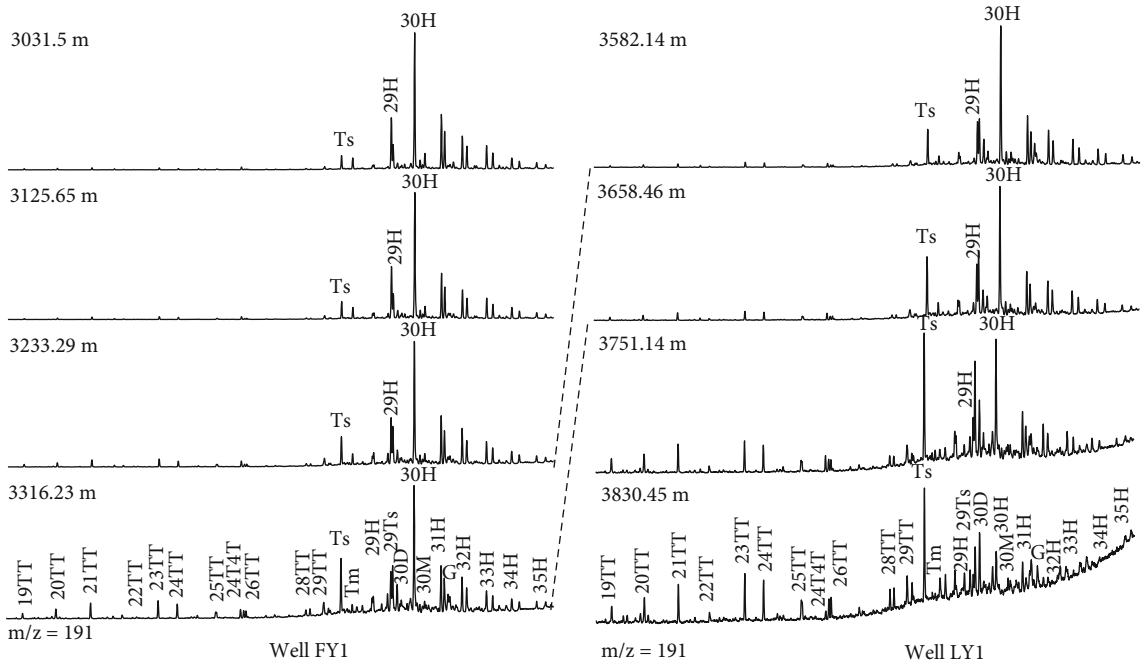

Figure 3: Mass chromatograms of m/z = 191 of the saturated hydrocarbon fraction showing the typical distribution of terpanes with increasing burial depth in wells FY1 and LY1. 19-29TT: C_{19}-C_{29} tricyclic terpanes; Ts:18α(H)-trisnorneohopane; Tm: 17α(H)-trisnorhopane; 29-35H: C_{29}-C_{35} 17α(H),21β(H) hopanes; 29Ts: 8α(H)-30-norneohopane; 30D: C_{30}-diahopane (15α-methyl-17α(H)-27-norhopane); 30 M: C_{30} 17β(H),21α(H)-hopane (moretane).

increasing burial depth in well LY1; however, ratio values are generally <0.05 in well NY1 and show no depth correlation (Figure 4(b)). Likewise, the $C_{29}Ts/(C_{29}Ts + C_{29}H)$ ratio values show a marked increase in wells FY1 (0.26–0.57) and LY1 (0.44–0.81) but less dramatic change and lower ratio values in NY1 (0.23–0.39) (Table 2).

Tricyclic terpanes are generally more abundant in highly mature oils and/or source rocks because they are thermally more stable than other terpanes, and thus the ratio of tricyclic terpanes to pentacyclic terpanes will rise with increasing maturity [15, 21]. The TT/(TT + PT) ratio values increase from 0.04 to 0.19 in FY1, from 0.04 to 0.13 in NY1, and from 0.08 to 0.46 in LY1, respectively (Figure 4(c)). Their evolution profiles are generally consistent with other maturity indicators, representing a successive maturity sequence in each well. This maturity indicator seems more useful for relatively mature bitumen than any of the others used in this study, as this ratio increases continuously during advanced stages of thermal maturation.

Distributions of steranes arranged by depth in wells FY1 and LY1 are shown in m/z 217 mass chromatograms (Figure 5). The regular steranes are dominated in majority samples, while pregnanes and diasteranes increase gradually with depth, especially in LY1. Similar to the response of hopanoids to increasing thermal stress, the stereochemical configuration of steranes departs from its biological configuration 5α(H),14α(H), 17α(H)-20R ($\alpha\alpha\alpha$-20R) to a mixture of $\alpha\alpha\alpha$-20S and $\alpha\beta\beta$-20R+20S [13]. On the basis of such evolution, two commonly used maturity parameters can be derived, i.e., $\alpha\alpha\alpha$ 20S/(20S + 20R) and $\beta\beta/(\beta\beta + \alpha\alpha)$. The C_{29} steranes are normally selected to avoid coelution issues. $C_{29}\alpha\alpha\alpha$ 20S/(20S + 20R) ratio in FY1 increases from 0.58 to 0.72 with increasing depth for the Es3 sample subset, while a slightly lower value of 0.70 occurs in one Es4 sample. One Es3 sample in NY1 has a $C_{29}\alpha\alpha\alpha$ 20S/(20S + 20R) ratio of 0.57, while these from the Es4 show a revered trend with depths decreasing from 0.67 to 0.47. Interestingly, the $C_{29}\alpha\alpha\alpha$ 20S/(20S + 20R) ratio values increase from 0.61 to 0.75 for the Es3 samples in LY1, but decrease from 0.70 to 0.55 for the Es4 samples (Figure 6(a)). The $C_{29}\alpha\alpha\alpha$ 20S/(20 S + 20R) ratio values in the studied samples are mostly approaching the equilibrium values (ca. 0.6 at Ro of 0.7%, Mackenzie, 1984). The $C_{29}\alpha\alpha\alpha$ 20S/(20S + 20R) ratio has lost the sensitivity as a maturity indicator in the studied sample suite.

The $C_{29}\beta\beta/(\beta\beta + \alpha\alpha)$ ratios in FY1 vary from 0.41 to 0.49 without depth correlation, while the ratio values increase consecutively from 0.35 to 0.59 in well NY1. The $C_{29}\beta\beta/(\beta\beta + \alpha\alpha)$ ratios for LY1 samples decreases from 0.51 to 0.49 in the Es3 source rocks but increases from 0.51 to 0.59 in the Es4, showing the opposite trend to $C_{29}\alpha\alpha\alpha$ 20S/(20S + 20R) ratios (Figure 6(b)). The $C_{29}\beta\beta/(\beta\beta + \alpha\alpha)$ ratio reaches the equilibrium point at a slightly higher maturity level (at R_o of 0.8%, Mackenzie [2]) than $\alpha\alpha\alpha$ 20S/(20S + 20R). However, the depth correlation of $C_{29}\beta\beta/(\beta\beta + \alpha\alpha)$ ratio has only been observed in well NY1, suggesting that samples from the other two wells have passed the equilibrium point. Both 20S/(20S + 20R) and β

Table 2: Maturity parameters derived from saturated and aromatic hydrocarbons.

Depth (m)	C_{31}S/R	C_{30}M/H	Ts/tm	C_{29}Ts/H	C_{30}D/H	TT/PT	C_{29}S/R	$C_{29}\beta\beta/\alpha\alpha$	DiaSt/St	TMNr	TeMNr	PMNr	MDR	MPI1	MPR	DMPR	TMPR	TA/MA	TASI
3031.5	0.58	0.11	0.54	0.29	0.05	0.04	0.58	0.46	0.22	0.49	0.48	0.18	2.11	0.45	0.80	0.93	0.28	0.74	0.14
3059.92	0.59	0.11	0.51	0.26	0.05	0.05	0.58	0.48	0.14	0.51	0.51	0.21	2.49	0.44	0.73	0.93	0.36	0.75	0.11
3125.65	0.57	0.09	0.61	0.31	0.07	0.06	0.61	0.45	0.16	0.57	0.61	0.22	2.67	0.44	0.67	0.97	0.56	0.76	0.21
3170.14	0.57	0.09	0.62	0.32	0.06	0.09	0.68	0.41	0.15	0.62	0.67	0.29	3.11	0.42	0.67	1.00	0.77	0.85	0.48
3233.29	0.57	0.09	0.72	0.41	0.10	0.11	0.72	0.46	0.17	0.68	0.68	0.38	5.01	0.47	0.76	1.35	1.53	0.78	0.46
3316.23	0.55	0.10	0.86	0.57	0.18	0.19	0.70	0.49	0.21	0.75	0.71	0.55	11.31	0.54	0.92	2.06	3.54	0.86	0.61
3304.1	0.59	0.13	0.43	0.25	0.03	0.04	0.57	0.39	0.17	0.47	0.46	0.11	1.40	0.36	0.53	0.89	0.22	0.80	0.09
3333.04	0.59	0.12	0.43	0.26	0.04	0.04	0.67	0.35	0.17	0.46	0.41	0.10	1.38	0.43	0.72	1.00	0.16	0.79	0.10
3372.9	0.59	0.12	0.48	0.27	0.03	0.05	0.57	0.44	0.15	0.50	0.49	0.18	3.47	0.44	0.78	1.00	0.37	0.73	0.11
3377.84	0.58	0.09	0.62	0.34	0.07	0.05	0.63	0.46	0.17	0.54	0.57	0.24	2.64	0.43	0.68	0.94	0.48	0.72	0.25
3402.73	0.59	0.10	0.47	0.23	0.03	0.06	0.54	0.45	0.16	0.48	0.49	0.14	3.52	0.42	0.73	0.95	0.32	0.82	0.15
3462.58	0.60	0.08	0.72	0.39	0.04	0.13	0.47	0.59	0.18	0.52	0.53	0.32	9.12	0.45	0.65	1.09	1.01	0.71	0.32
3582.14	0.57	0.08	0.78	0.50	0.15	0.08	0.61	0.51	0.20	0.66	0.61	0.38	3.13	0.52	0.78	1.29	1.15	0.62	0.34
3586.16	0.57	0.07	0.75	0.47	0.13	0.08	0.59	0.51	0.17	0.67	0.61	0.38	3.11	0.51	0.77	1.29	1.20	0.63	0.35
3593.01	0.57	0.04	0.73	0.44	0.12	0.08	0.59	0.50	0.17	0.68	0.65	0.39	3.04	0.51	0.78	1.45	1.39	0.63	0.38
3598.15	0.57	0.09	0.71	0.44	0.11	0.09	0.59	0.50	0.16	0.69	0.67	0.42	3.20	0.51	0.77	1.36	1.47	0.67	0.40
3601.21	0.57	0.09	0.71	0.44	0.11	0.09	0.60	0.51	0.16	0.70	0.68	0.40	3.20	0.52	0.77	1.43	1.51	0.64	0.39
3658.46	0.56	0.09	0.80	0.57	0.17	0.13	0.75	0.42	0.21	0.78	0.75	0.53	4.28	0.54	0.79	1.87	2.77	0.71	0.62
3672.38	0.57	0.08	0.82	0.56	0.17	0.13	0.74	0.44	0.22	0.79	0.75	0.46	4.95	0.55	0.81	2.60	3.51	0.80	0.65
3674.34	0.58	0.08	0.81	0.60	0.17	0.14	0.73	0.44	0.22	0.81	0.74	0.49	4.70	0.55	0.84	2.42	3.43	0.79	0.64
3751.14	0.53	0.11	0.92	0.70	0.32	0.24	0.66	0.51	0.29	0.83	0.71	0.42	10.67	0.61	1.03	3.99	5.34	0.77	0.80
3768.15	0.52	0.10	0.95	0.76	0.42	0.28	0.66	0.56	0.31	0.81	0.68	0.38	14.27	0.63	1.02	3.98	7.55	0.75	0.79
3771.81	0.56	0.10	0.95	0.76	0.42	0.29	0.70	0.51	0.31	0.82	0.71	0.41	17.37	0.63	1.02	4.15	7.55	0.76	0.78
3786.16	0.57	0.32	0.95	0.75	0.50	0.38	0.64	0.53	0.35	0.81	0.68	0.45	20.45	0.63	1.02	4.19	7.88	0.79	0.83
3803.65	0.61	0.15	0.94	0.81	0.63	0.46	0.63	0.59	0.31	0.82	0.71	0.47	22.56	0.64	0.99	4.68	8.57	0.81	0.78
3815.76	0.63	0.11	0.94	0.77	0.58	0.45	0.67	0.54	0.35	0.82	0.71	0.42	17.35	0.65	0.99	5.74	7.47	0.75	0.80
3830.45	0.60	0.10	0.94	0.69	0.54	0.43	0.55	0.57	0.39	0.83	0.72	0.43	14.18	0.65	0.99	5.36	6.82	0.74	0.79

C_{31}S/R: C_{31} 22S/22 (S + R); C_{30}M/H: $C_{30}\beta\alpha$ hopane/$C_{30}\alpha\beta$ hopane; Ts/Tm: Ts/(Ts + Tm); C_{29}Ts/H: C_{29}Ts/(C_{29}Ts + C_{29}H); C_{30}D/H: C_{30}D/(C_{30}D + C_{30}H); TT/PT: ∑tricyclic terpanes/(∑tri−+pentacyclic terpanes); C_{29}S/R: C_{29} steranes 20S/(S + R); $C_{29}\beta\beta/\alpha\alpha$: C29 steranes $\beta\beta/(\alpha\alpha + \beta\beta)$; DiaSt/St: diasteranes/(diasteranes + steranes); MNR: 2-MN/1-MN; DNR: (2,6-DMN+ 2,7-DMN)/1,5-DMN; TMNr: 1, 3, 7 − TMN/(1,3,7−+1, 2, 5 − TMN); TeMNr: 1, 3, 6, 7 − /(1,3,6,7−+1,2,5,6 + 1, 2, 3, 5 − TeMN); PMNr: 1, 2, 4, 6, 7 − /(1,2,4,6,7−+1, 2, 3, 5, 6 − PMN); MDR: 4-MDBT/1-MDBT; MPI1: 1.5 × (2 − MP + 3 − MP)/(P + 1 − MP + 9 − MP); MPR: 2-MP/1-MP; DMPR: 2,7-DMP/1,2-DMP; TMPR = 1,6,9 − +1,7,9−+2, 3, 7 − TMP/1, 2, 8 − TMP; TA/MA: TAS/(TAS + MAS); TASI : C20 − 21/(C20 + C21 + C28) − TAS.

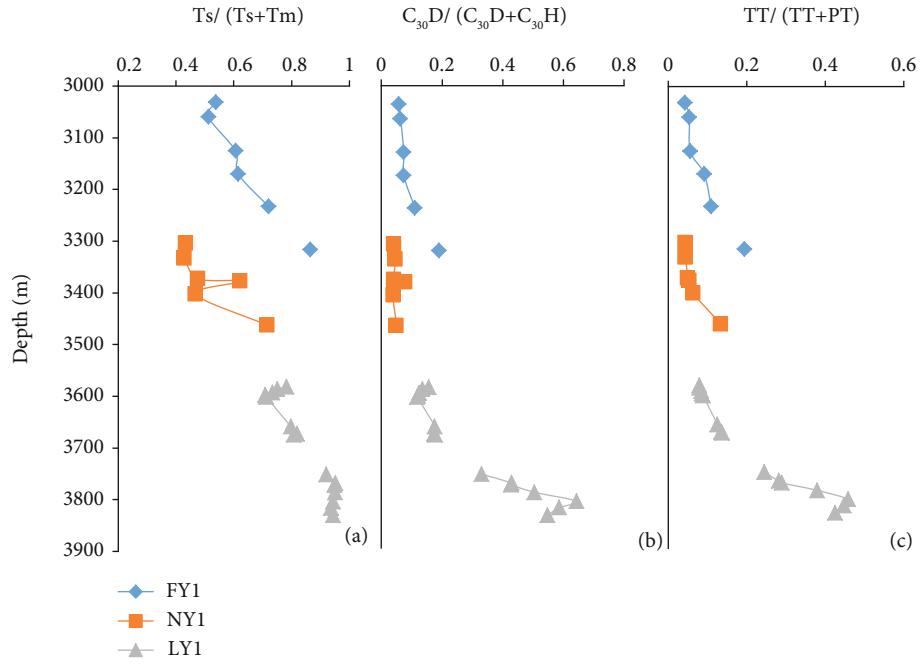

Figure 4: Maturity profile derived from terpanes in the 3 studied wells. (a) Ts/(Ts + Tm). (b) $C_{30}D/(C_{30}D + C_{30}H)$. (c) TT/(TT + PT).

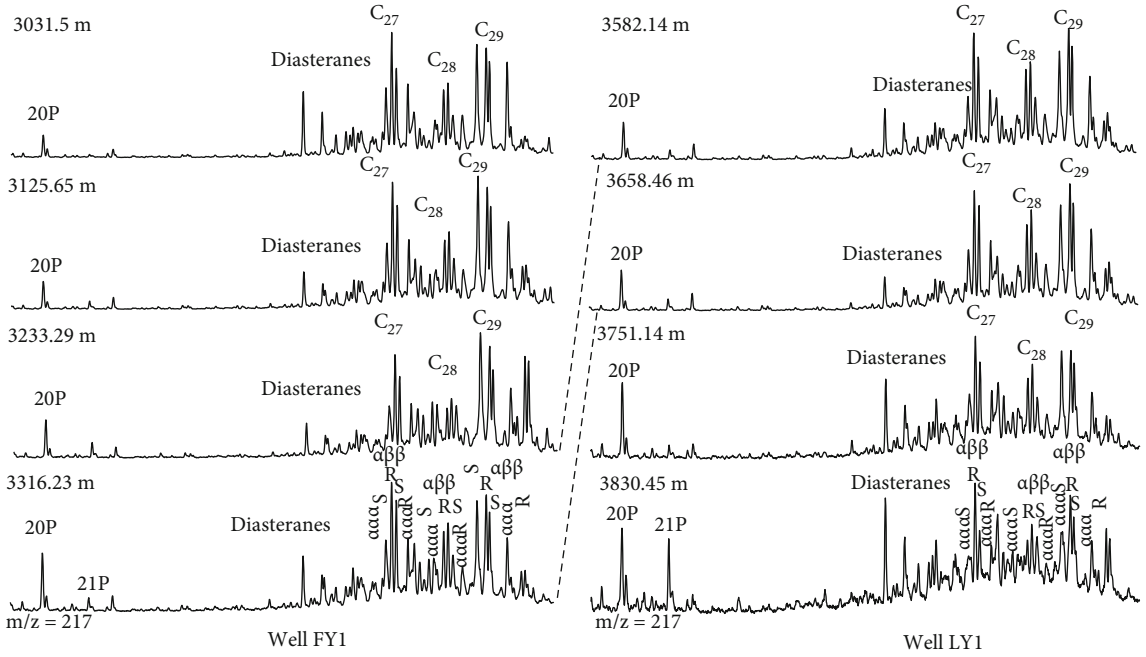

Figure 5: Mass chromatograms of m/z = 217 of the saturated hydrocarbon fraction showing the typical distribution of steranes with increasing burial depth in wells FY1 and LY1. 20-21P: C_{20}-C_{21} pregnanes; ααα S: 5α(H),14α(H),21α(H),20S; αββ R: 5α(H),14β(H),21β(H),20R; αββ S: 5α(H),14β(H),21β(H),20S; ααα R: 5α(H),14α(H),21α(H),20R.

$\beta/(\beta\beta + \alpha\alpha)$ ratios will be reversed at the peak oil generation stage [15] and are not sensitive to maturity variation in the studied samples.

The diasteranes/steranes ratio is also maturity-related indicator as diasteranes are thermally more stable than regular steranes, which increases after the peak oil generation window [13]. The ratios $C_{27\text{-}29}$ diasteranes to $C_{27\text{-}29}$ regular steranes [DiaSt/(DiaSt+St)] vary in a narrow range of 0.14–0.25 in wells FY1 and NY1 without a clear depth trend, but increase continuously from 0.17 to 0.39 in well LY1 (Figure 6(c)), suggesting that the diasteranes/steranes ratio is a valid maturity indicator for studied sample suite.

Concentrations of all biomarkers decrease with increasing maturity and can more accurately reflect maturity

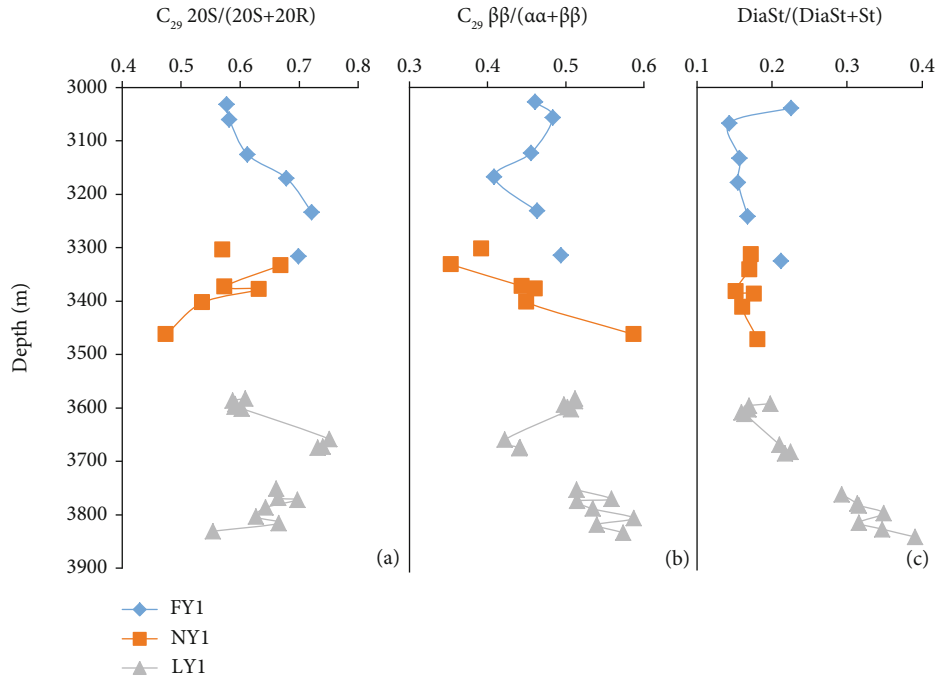

Figure 6: Maturity profile derived from steranes in the 3 studied wells. (a) $C_{29}\alpha\alpha\alpha$ 20S/(20S + 20R). (b) $C_{29}\alpha\beta\beta/(\alpha\beta\beta + \alpha\alpha\alpha)$. (c) Diasteranes/(diasteranes + regular steranes).

variation [21]. Summed concentrations of three typical biomarker compound classes, expressed relative to the mass of extractable organic matter, were plotted in Figure 7. Concentrations of $C_{19\text{-}30}$ tricyclic terpanes vary from 470 to 1100 μg/g EOM (ppm) in well FY1 and these in wells NY1 and LY1 from 650 to 1330 ppm and from 160 to 770 ppm, respectively. While the data are scattered and fluctuated in each well, a clear decrease trend with increasing depth can be illustrated (Figure 7(a)). More dramatic concentration variations can be observed in the pentacyclic terpanes, which decrease from 18,700 to 1,900 ppm, from 27,000 to 4,200 ppm, and from 8,200 to <300 ppm with increasing burial depths in wells FY1, NY1, and LY1, respectively (Figure 7(b)). Clearly, the concentrations of both tri- and pentacyclic terpanes decrease with increasing depth (thermal maturity) but at different rates. More abrupt depletion of pentacyclic terpanes than tricyclic terpanes results in the rise of TT/PT ratio rather than a formation of tricyclic terpanes from pentacyclic terpanes.

Concentrations of $C_{27\text{-}29}$ regular steranes decrease from about 3,000 ppm to 600 ppm with increasing depth in well FY1 and from 1,700 ppm to 150 ppm in well LY1. However, no depletion trend with increasing depth has been observed in NY1 with the highest amount of 4,100 ppm occurring in the deepest sample (Figure 7(c)). This further verifies that well NY1 suffers less extensive thermal stress than wells FY1 and LY1.

4.3. Maturity Indicators Derived from Aromatic Hydrocarbons. Occurrence and behavior of polyaromatic hydrocarbons (PAHs) have been thoroughly investigated in organic geochemistry. It has long been recognized that the abundance and distribution of PAHs and their structural isomers can be used to assess the maturation of source rock, bitumens, and oils, especially at high maturity levels [41–43]. The alkylated naphthalenes, phenanthrenes, and dibenzothiophenes are common constituents of oils and source rock extracts. During maturation, thermally less stable forms in the α-position will be transferred to thermally more stable forms in the β-position, and the β/α ratio for particular groups of compounds can be used as a maturity indicator [42–45]. Numerous maturity parameters based on these compounds are available in literature, but only a few commonly used ones have been explored in the present study.

Representative mass chromatograms of m/z = 170 + 184 + 198 show the distributions of C3-, C4-, and C5-alkylnaphthalenes, dibenzothiophene and methyldibenzothiophenes in source rock extracts at wells FY1 and LY1 (Figure 8). Based on thermodynamic considerations, the most thermally stable trimethylnaphthalene (TMN) isomer is 2,3,6-TMN, and one of the least stable isomers is 1,2,5-TMN, which is often abundant in low maturity oil samples. The depletion of the relative abundance of 1,2,5-TMN can be visually observed from both columns. van Aarssen et al. [45] defined trimethylnaphthalene ratio (TMNr) as $1,3,7 - \mathrm{TMN}/(1,3,7 - + 1,2,5 - \mathrm{TMN})$. The ratio values increase almost linearly with depth from 0.49 to 0.75 in FY1, from 0.46 to 0.54 in well NY1, and from 0.66 to 0.83 in LY1 (Figure 9(a), Table 2).

Among the tetramethylnaphthalenes (TeMN), 1,3,6,7-TeMN is the most thermally stable isomer, whereas 1,2,5,6-TeMN is the least thermally stable and usually the most abundant isomer in samples of low maturity. Decrease of 1,2,5,6-TeMN against other tetramethylnaphthalenes with increasing depth can be clearly seen in both wells. Under the chromatographic conditions used in the present study,

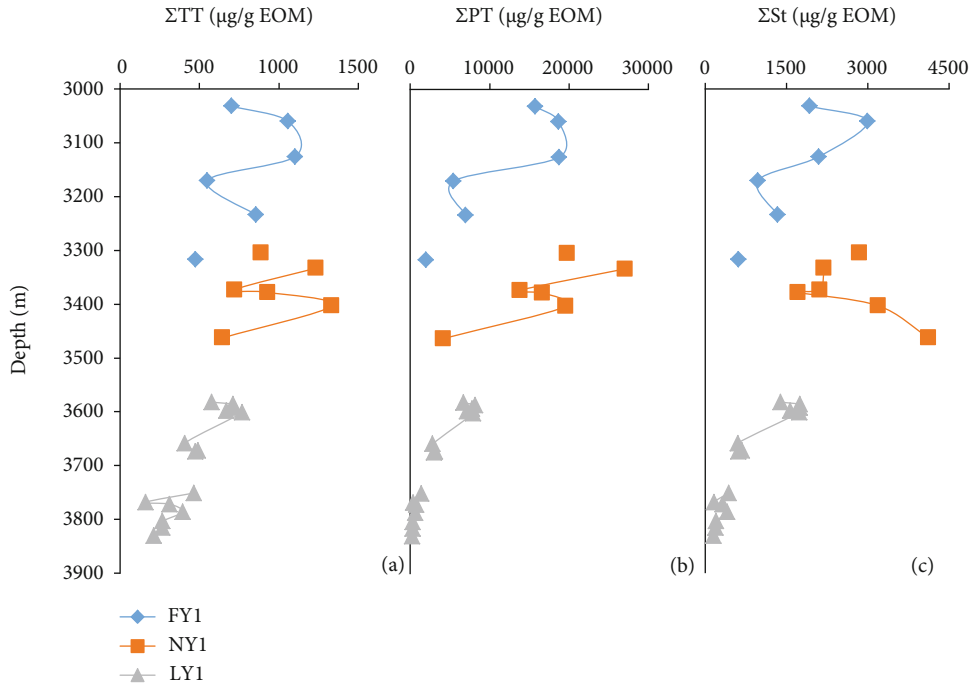

Figure 7: Biomarker concentration variations in the 3 studied wells. (a) Summed tricyclic terpanes (TT). (b) Summed pentacyclic terpanes (PT). (c) Summed regular steranes (St).

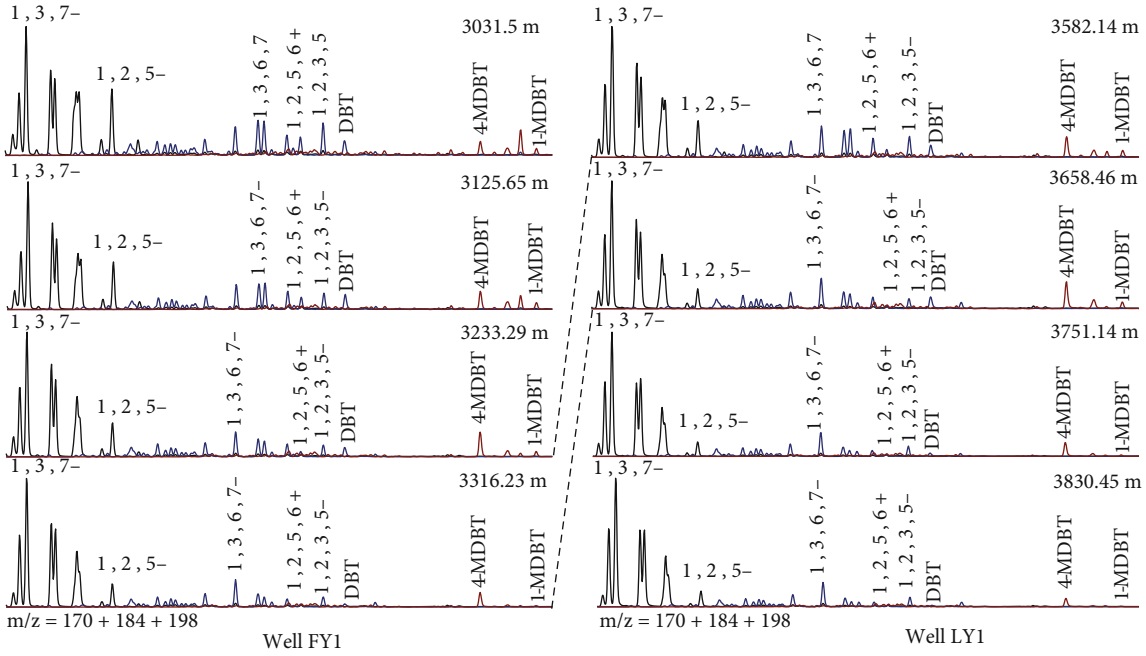

Figure 8: Mass chromatograms of m/z = 170 + 184 + 198 of the aromatic hydrocarbon fraction showing the typical distribution of C3–C5-alkylnaphthalenes, dibenzothiophene (DBT), and methyldibenzothiophenes (MDBT) with increasing burial depth in wells FY1 and LY1.

1,2,5,6-TeMN is coeluted with 1,2,3,5-TeMN, which is very similar in stability to each other. van Aarssen et al. [45] defined the ratio of 1,3,6,7-TeMN to the sum of 1,3,6,7-TeMN and (1,2,5,6 + 1,2,3,5)-TeMN as tetramethylnaphthalene ratio (TeMNr). Ratio values of TeMNr increase from 0.48 to 0.71 in FY1, from 0.41 to 0.57 in NY1, and from 0.61 to 0.75 in LY1 (Figure 9(b), Table 2). Both TMNr and TeMNr have high coefficient with Ts/(Ts + Tm) (> 0.75) (Table 2), therefore to be the most suitable maturity indicators among alkylnaphthalenes.

The thermal stability of alkyldibenzothiophenes varies with the position of substitution. A shift from a thermally

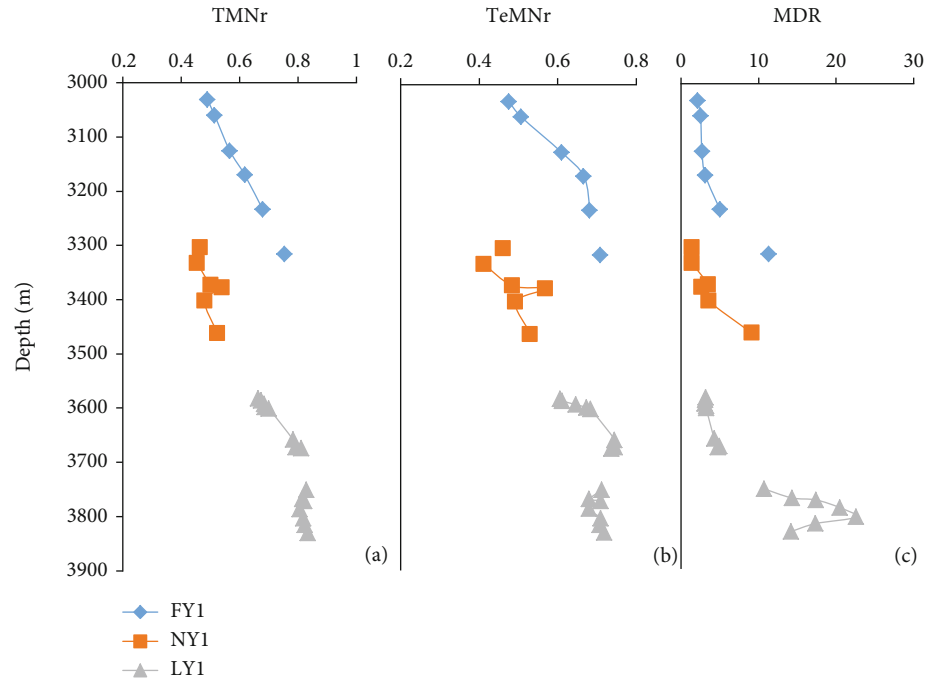

Figure 9: Maturity profile derived from alkylnaphthalenes and alkyldibenzothiophenes in the 3 studied wells. (a) Trimethylnaphthalene ratio (TMNr). (b) Tetramethylnaphthalene ratio (TeMNr). (c) Methyldibenzothiophene ratio (MDR).

less stable 1-methyldibenzothiophene (1-MDBT) towards a more stable 4-MDBT on maturation forms another commonly used maturity indicator, methyldibenzothiophene ratio (MDR = 4 − MDBT/1 − MDBT, Radke et al. [46]). The MDR values increase from 2.1 to 11.3 in FY1, from 1.4 to 9.1 in NY1, and from 3.1 to 22.6 in LY1, respectively (Figure 9(c), Table 2). Lower MDR value in NY1 than the other two wells indicates lower maturity levels.

Representative mass chromatograms of m/z = 178 + 192 + 206 + 220 show the distribution of C0-3-alkylphenanthrenes in wells FY1 and LY1 (Figure 10). While less dramatic than alkylnaphthalenes, systematic changes in alkylphenanthrene composition with increasing burial depth still can be observed. Radke and Welte [41] observed that the relative amounts of 2- and 3-methylphenanthrene (MP) increase compared to the 1- and 9-MP isomers with increasing burial depth and proposed the methylphenanthrene index
[MPI1 = 1.5 × (2 − MP + 3 − MP)/(P + 1 − MP + 9 − MP)].
The MPI1 values in wells FY1, NY1, and LY1 are in the range of 0.42–0.54, 0.36–0.45, and 0.51–0.65, respectively, and increase with burial depth (Figure 11(a), Table 2). Similar change can be observed in methylphenanthrene ratio (MPR = 2 − MP/1 − MP), which increased from 0.67 to 0.92, 0.53 to 0.78, and 0.77 to 1.03 in wells FY1, NY1, and LY1, respectively (Table 2).

Distribution of C2-alkylphenanthrene isomers is also sensitive to thermal maturation. 2,7-dimethylphenanthrene (DMP) is one of the most stable isomers, while 1,2-DMP is one of the least stable isomers. Ratio of 2,7-DMP/1,2-DMP proposed as dimethylphenanthrene ratio (DMPR, Radke [43]) in the present study, which increase linearly with depths from 0.93 to 2.06 in FY1, from 0.89 to 1.09 in well NY1, and from 1.29 to 5.74 in well LY1, respectively (Figure 11(b), Table 2).

Maturity influence on the distribution of C3-alkylphenanthrene isomers has not been illustrated in the literature. The correlation of the relative abundance of individual isomers with burial depth suggests that the coeluted peak containing 1,6,9- + 1,7,9- + 2,3,7-trimethylphenanthrene (TMP) is the most stable one while 1,2,8-TMP is the least stable one. The trimethylphenanthrene ratio (TMPR = 1,6,9−+1,7,9−+2, 3, 7 − TMP/1, 2, 8 − TMP) shows very similar trend as MDR and can be served as novel maturity parameter. The lowest TMPR value in NY1 is consistent with many other maturity parameters and suggests the lowest maturity level in the three studied wells (Figure 11(c), Table 2).

The m/z = 253 and 231 mass chromatograms display the distributions of mono- and triaromatic steroids identified from the aromatic fraction of the studied source rocks. The monoaromatic steroids appear in relatively low abundance compared to triaromatic steroids (Figure 12). The former is mainly present in immature organic matter, while the latter may form in organic matter at a later stage of diagenesis. Under thermal stress, steroids undergo irreversible aromatization and side chain cleavage, and their distribution and concentrations are commonly used to assess the thermal maturity of sedimentary organic matter [47].

Two widely used parameters can be derived from aromatic steroids. The degree of steroid hydrocarbon aromatization [TA/(TA + MA)] (TA is total triaromatic steroid hydrocarbons, and MA is total monoaromatic steroid hydrocarbons) is one of the commonly used maturity

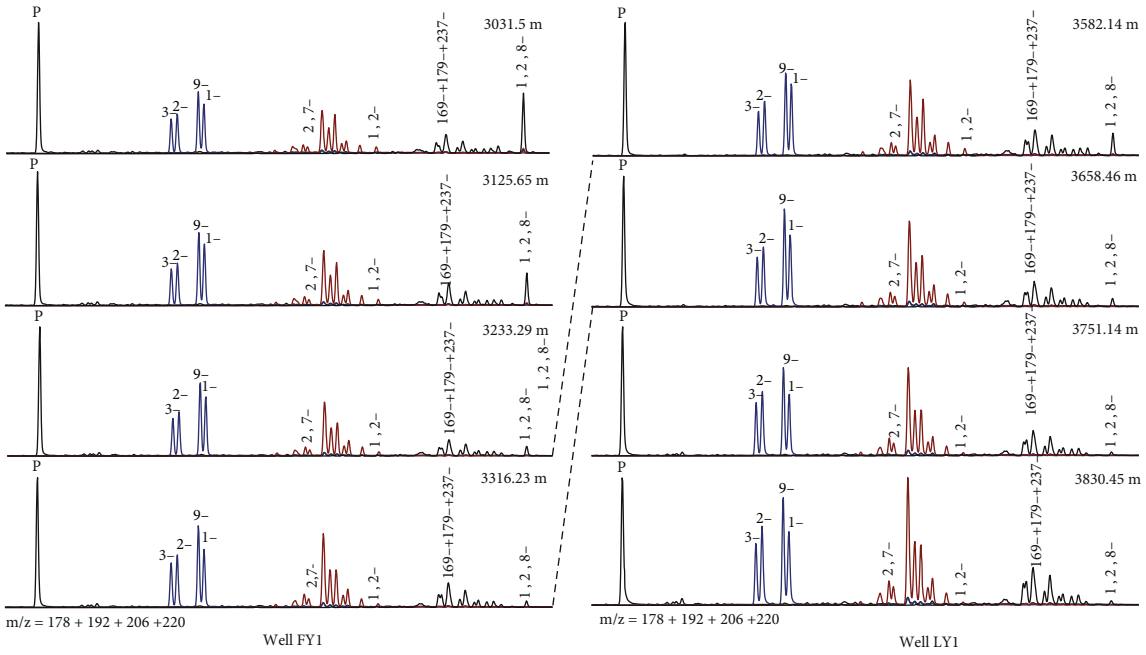

Figure 10: Mass chromatograms of m/z = 178 + 192 + 206 + 220 of the aromatic hydrocarbon fraction showing the typical distribution of C0-C3-alkylphenanthrenes with increasing burial depth in wells FY1 and LY1.

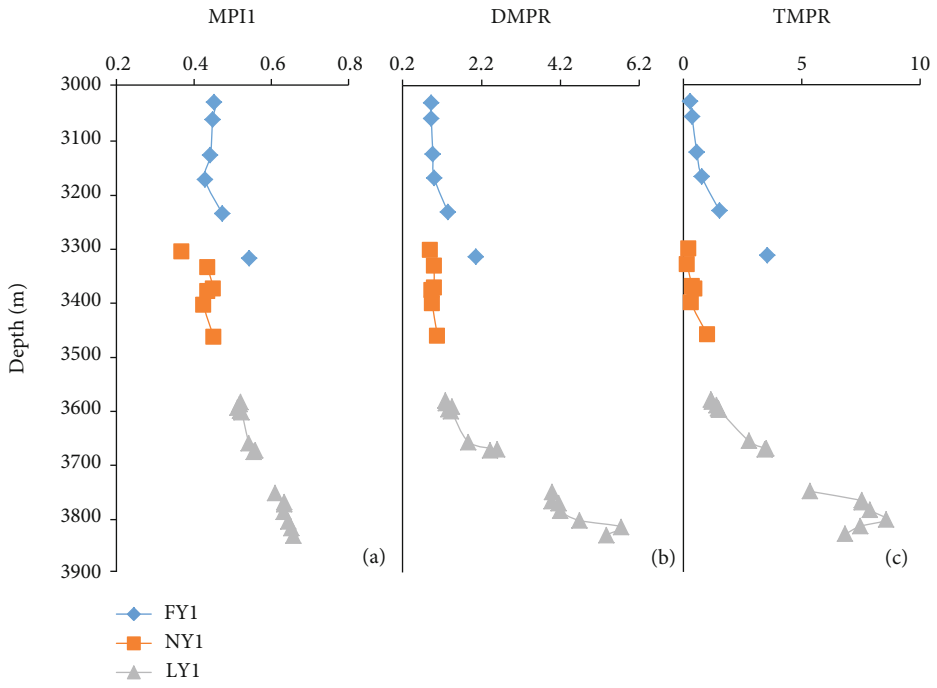

Figure 11: Maturity profile derived from alkylphenanthrenes in the 3 studied wells. (a) Methylphenanthrene Index 1 (MPI1). (b) Dimethylphenanthrene ratio (DMPR). (c) Trimethylphenanthrene ratio (TMPR).

parameters. Monoaromatic steroid hydrocarbons are believed to be converted to triaromatic steroid hydrocarbons during maturation. However, the TA/(MA + TA) ratio did not change accordingly in the studied wells (Table 2). This parameter seems only valid at the early oil generation window, but the present studied samples are already in the oil generation window. Another widely used parameter is the ratio of short side-chain triaromatic steroid hydrocarbons to long side-chain components, which increase with increasing maturity [47]. The long-chain triaromatic steroids are extremely enriched in low mature samples, while the short-chained ones are gradually enriched in the highly matured

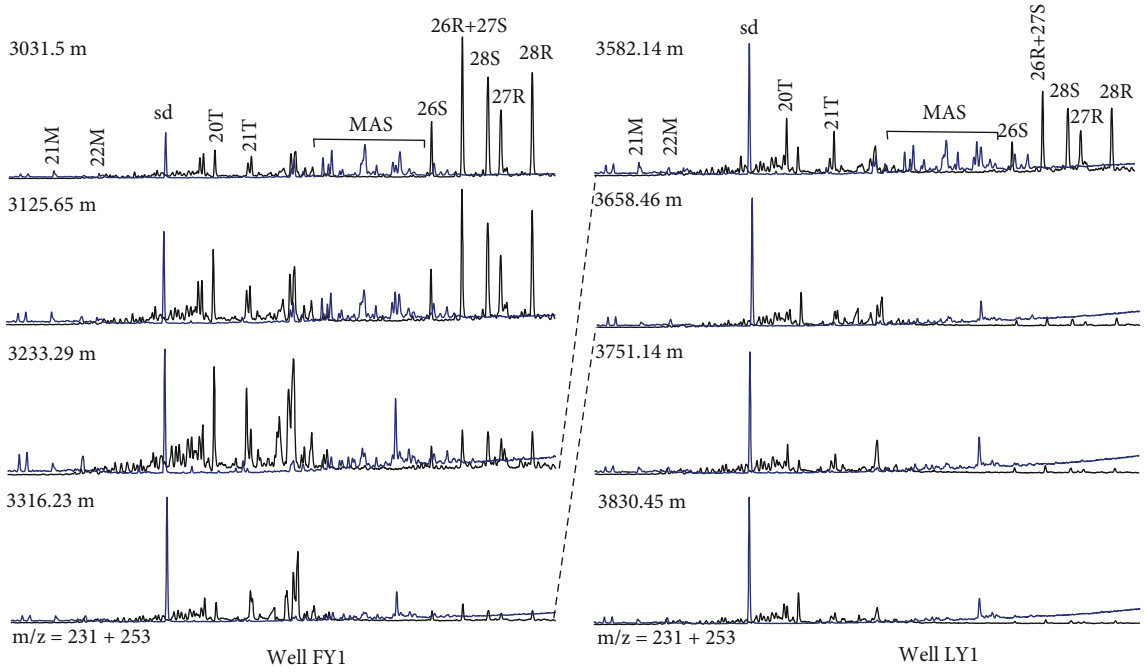

Figure 12: Mass chromatograms of m/z = 231 + 253 of the aromatic hydrocarbon fraction showing the typical distribution of mono- and triaromatic steroid hydrocarbons with increasing burial depth in wells FY1 and LY1. 21-22 M: C_{21}-C_{22} monoaromatic steroids; 20-21 T: C_{20}-C_{21} triaromatic steroids; 26-28R/S: C_{26}-C_{28} triaromatic steroids; sd: internal standard.

samples. The ratios of short chain triaromatic steroids (C_{20}–C_{21}) to the sum of short plus C_{28} triaromatic steroids [$C_{20–21}/(C_{20} + C_{21} + C_{28})$ – TAS] increase from 0.11 to 0.61 in FY1, from 0.09 to 0.32 in well NY1, and from 0.34 to 0.83 in well LY1 (Figure 13(a), Table 2).

The concentrations of monoaromatic steroids decrease sharply from 450 ppm at the top to < 10 ppm at the bottom in FY1. However, only a gentle decrease has been observed in NY1 where the concentrations of monoaromatic steroids vary between 210 and 470 ppm. The concentrations of monoaromatic steroids decreases sharply from 165 ppm at 3582 m to less than 10 ppm at 3672 m LY1, and no reliable monoaromatic steroids can be quantified in samples deeper than 3672 m (Figure 13(b)). Concentrations of triaromatic steroids show the same evolution trajectories as these of monoaromatic steroids (Figure 13(c)).

5. Discussion

In the case of the Dongying Depression, the measured vitrinite reflectance values may not represent the actual maturity level due to suppression [27, 30], while the degree of suppression has not been elucidated [48]. Similarly, the molecular maturity parameters are also not universally valid because the relative roles of time and temperature can vary among the various biomarker transformations [2], and they are susceptible to variation in organofacies [15]. They permit the recognition and definition of maturity levels in a relative sense. Nevertheless, both vitrinite reflectance and molecular parameters illustrated the same maturity discrepancy in different wells. The assumption of a uniform thermal gradient across the whole depression needs revisit.

Actually, a variable maturity-depth trend has been noticed by previous investigations. Rock-Eval pyrolysis production index and borehole temperatures of well FY1 deviating from the average geothermal gradient have been noticed by Ping et al. [30], and they suggested that the source rock in well FY1 started oil generation earlier than that of other wells. Similarly, Guo et al. [27] recognized that the oil generation related overpressured zone top in the southern part of the Dongying Depression is shallower than that in the northern part. However, those phenomena have been ignored in their regional studies. Samples in the present study show a systematic maturity-depth correlation in each well. The maturity differences at the same depth in different wells are most likely caused by different thermal regimes at different sags where 3 wells are situated. Variable threshold depths in different studies likely echo the variable thermal gradients, while different methods inevitably exert some impact on the evaluation results. Geothermal gradient and/or temperature variation in space and time depends on both the heat flow and thermal conductivity of the basin, which are functions of tectonic settings and lithology [49]. While lithology variation results in variable conductivity in different depositional systems, the samples studied here are largely from the same stratigraphic unit and have very similar lithologies. No robust evidence indicates that large lithological facies variations occurs in the Dongying Depression, which can result in the observed maturity-depth trend, while further investigation is still called for. We suggest that the variation of heat flow plays a critical role for variable maturity levels across depression.

Early measurements have illustrated that heat flow varies from 60 mW/m^2 in the deep depocentres to > 70 mW/m^2 in

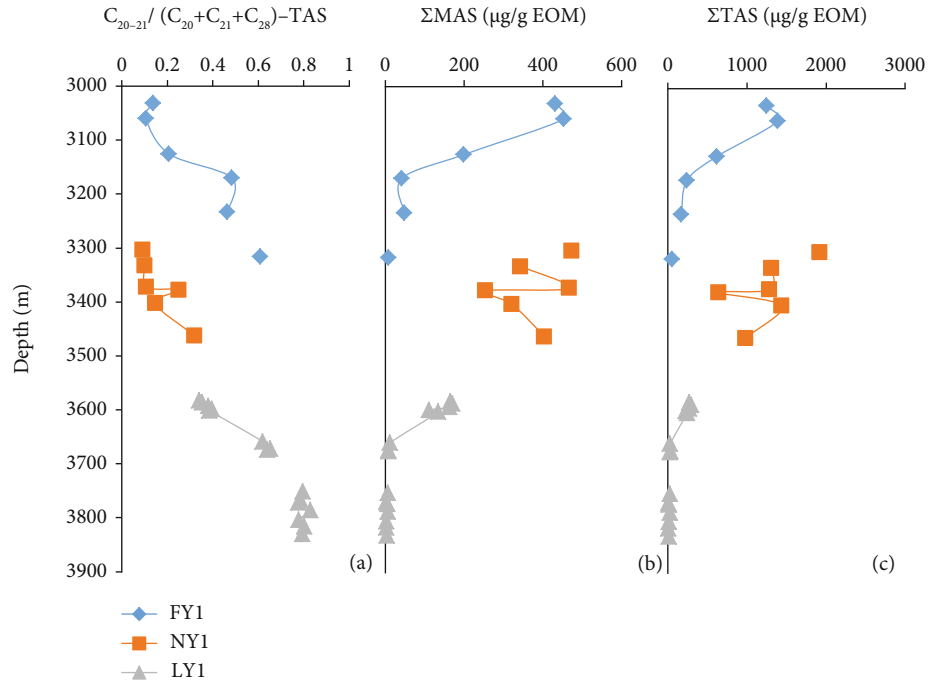

Figure 13: Thermal evolution of mono- and triaromatic steroid hydrocarbons in the 3 studied wells. (a) $C_{20-21}/(C_{20} + C_{21} + C_{28})$ – TAS. (b) Summed concentration of C_{27}-C_{29} monoaromatic steroids. (c) Summed concentration of C_{26}-C_{28} triaromatic steroids.

the uplifts in the Jiyang subbasin [50]. Geographically, the highest thermal gradient occurs in the Dongying Depression, followed by the Zhanhua and Huimin depressions, and the lowest in the Chezhen Depression [51]. Therefore, the threshold depth of hydrocarbon generation in the Dongying Depression is shallower than other depressions. Within the Dongying Depression, current heat flow values in wells Liang-70 and Shi-115 are 65.2 mW/m^2 and 59.5 mW/m^2, respectively [28]. While variable heat flow is a common phenomenon in the Bohai Bay Basin [52] and it occurs in the Dongying Depression, a uniform thermal gradient has been assumed with an average geothermal gradient of 36.0°C/km and a constant heat flow of 60 mW/m^2 [28] or an average geothermal gradient of 35.0°C/km and a constant heat flow of 61 mW/m^2 [32] in practical applications. Indeed, the assumption of a uniform geothermal gradient across the whole depression conflicts with the abovementioned observations.

Heat flow variation exerts a variable impact on the thermal evolution of organic matter in sedimentary basins [53]. The Bohai Bay Basin was formed as a typical rift basin but was modified by synchronous strike-slip deformation. The strike-slip of the Tanlu Fault began at the middle stage of deposition of the Shahejie Formation and reached its climax during deposition of the Dongying Formation, which exerts significant impacts on the structural framework of the Bohai Bay Basin [31, 54]. While the hydrothermal fluid interference is difficult to verify in the present study due to limited data availability, the heat transport along basement faults during the rift stage creates different thermal regimes in different depressions. Higher thermal gradient in the Dongying Depression than other depressions in the Jiyang subbasin is due to its relative shorter distance to the Tanlu Fault. The dependence on the distance to the Tanlu Fault plays a role within the Dongying Depression as well. Higher levels of maturity could be reached at the southern side of the Dongying Depression than those at the northern side due to the variable distance towards the Tanlu Fault. Well FY1 is situated mostly close to the Tanlu Fault while well LY1 is located mostly away from the Tanlu Fault. Therefore, the same maturity level indicated by vitrinite reflectance and various molecular parameters in well FY1 is about 300 m shallower than that in well NY1 and 500 m shallower than that in well LY1. Variable geothermal gradients rather than an overall average gradient should be used for the respective unit intervals. The variable hydrocarbon generation threshold depths defined by previous studies can partially be attributed to variable thermal gradients at different locations. Wide range variations of measured vitrinite reflectance (0.2–0.3%) within short burial depth (200–300 m) may reflect either hydrothermal fluid interference or the transition from suppressed interval to the normal trend line [30]. Variable hydrocarbon generation thresholds illustrated by molecular compositions and petrological measurement in the present study provide a practical guideline for exploration perspective within the Dongying Depression, especially shale oil and sweetspot assessment.

6. Conclusion

Core samples from the Eocene Shahejie Formation in wells FY1, NY1, and LY1 of the Dongying Depression show systematical burial depth-related maturity trends. The molecular compositions derived from extractable organic matter yield internally consistent thermal maturity with vitrinite reflectance (%R_o). The measured R_o values lie in the range

of 0.5–0.9%, indicating early mature to moderately mature conditions, while molecular ratios including hopane and sterane rearrangement, aromatic hydrocarbon isomerization, and steroid thermal cracking suggest a slightly higher maturity level. The same maturity appearance in well FY1 situated at the southern side of the Dongying Depression is about 300 m shallower than that in well NY1 located at the middle of the depression and 500 m shallower than that in well LY1 located at the northern side of the depression. The variation in hydrocarbon generation threshold depth across the Dongying Depression is caused by the different thermal regimes that each well has experienced. The systematic variability of maturity with geographic position along the depression is a dependence on the distance towards the Tanlu Fault front in the south of the Dongying Depression. Sufficiently high heat flow in the southern side of the depression may have important implications for the timing of hydrocarbon maturation and expulsion, particularly for the shale oil interval where maturity plays a critical role for the mobility of oil.

Data Availability

Most data are already included in the text. More details regarding GC-MS raw data are avaiable upon request.

Conflicts of Interest

The authors declare that they have no conflicts of interest.

Acknowledgments

This study is supported by the National Natural Science Foundation of China (Grant Number 41873049). Prof. Steve Larter from University of Calgary and two anonymous reviewers are acknowledged for their constructive comments, which improve the quality of this manuscript substantially.

References

[1] D. K. Baskin, "Atomic H/C ratio of kerogen as an estimate of thermal maturity and organic matter conversion," *AAPG Bulletin*, vol. 81, pp. 1437–1450, 1997.

[2] A. S. Mackenzie, "Application of biological markers in petroleum geochemistry," in *Advances in Petroleum Geochemistry I*, J. Brooks and D. Welte, Eds., pp. 115–214, Academic Press, London, 1984.

[3] I. Atwah, S. Sweet, J. Pantano, and A. Knap, "Light hydrocarbon geochemistry: insight into Mississippian crude oil sources from the Anadarko Basin, Oklahoma, USA," *Geofluids*, vol. 2019, Article ID 2795017, 15 pages, 2019.

[4] R. Bertrand and Y. Heroux, "Chitinozoan, graptolite, and scolecodont reflectance as an alternative to vitrinite and pyrobitumen reflectance in Ordovician and Silurian strata, Anticosti Island, Quebec, Canada," *AAPG Bulletin*, vol. 71, pp. 951–957, 1987.

[5] C. E. Barker and M. J. Pawlewicz, "Calculation of vitrinite reflectance from thermal histories and peak temperatures: a comparison of methods," in *Vitrinite Reflectance as a Maturity Parameter, Applications and Limitations*, P. K. Mukhopadhyay and W. G. Dow, Eds., vol. 570, pp. 216–229, American Chemical Society Symposium Series, Washington, DC, 1994.

[6] J. J. Sweeney and A. K. Burnham, "Evaluation of a simple model of vitrinite reflectance based on chemical kinetics," *AAPG Bulletin*, vol. 74, pp. 1559–1570, 1990.

[7] S. Jiang, Y. Zuo, M. Yang, and R. Feng, "Reconstruction of the Cenozoic tectono-thermal history of the Dongpu Depression, Bohai Bay Basin, China: Constraints from apatite fission track and vitrinite reflectance data," *Journal of Petroleum Science and Engineering*, vol. 205, article 108809, 2021.

[8] S. Kumar and K. Ojha, "Reaction kinetic, maturity, burial and thermal histories modelling of cambay shale source rocks, Cambay Basin, Western India," *Journal of Petroleum Science and Engineering*, vol. 202, article 108543, 2021.

[9] P. K. Mukhopadhyay, "Vitrinite reflectance as maturity parameter – petrographic and molecular characterization and its applications to basin modeling," in *ACS Symposium Series*, vol. 570, pp. 1–24, American Chemical Society, 1994.

[10] K. E. Peters, "Guidelines for evaluating petroleum source Rock using programmed pyrolysis," *AAPG Bulletin*, vol. 70, pp. 318–329, 1986.

[11] L. R. Snowdon, "Rock–Eval Tmax suppression: documentation and amelioration," *AAPG Bulletin*, vol. 79, pp. 1337–1348, 1995.

[12] Z. Chen, K. Dewing, D. P. Synnott, and X. Liu, "Correcting T_{max} Suppression: a numerical model for removing adsorbed heavy oil and bitumen from upper Ordovician source rocks, Arctic Canada," *Energy & Fuels*, vol. 33, no. 7, pp. 6234–6246, 2019.

[13] W. K. Seifert and J. M. Moldowan, "Use of biological markers in petroleum exploration," in *Biological Markers in the Sedimentary Record 24, Methods in Geochemistry and Geophysics*, R. B. Johns, Ed., pp. 261–290, Elsevier, 1986.

[14] Q. Wang, H. Huang, Z. Li, and Z. X. Li, "Novel thermal maturity parameters derived from alkylbiphenyls and alkyldiphenylmethanes," *Energy & Fuels*, vol. 33, no. 9, pp. 8491–8502, 2019.

[15] D. W. Waples and T. Machihara, "Application of sterane and triterpane biomarkers in petroleum exploration," *Bulletin of Canadian Petroleum Geology*, vol. 38, pp. 357–380, 1990.

[16] A. N. Bishop and G. D. Abbott, "Vitrinite reflectance and molecular geochemistry of Jurassic sediments: the influence of heating by Tertiary dykes (northwest Scotland)," *Organic Geochemistry*, vol. 22, no. 1, pp. 165–177, 1995.

[17] P. Farrimond, A. Taylor, and N. Telnaes, "Biomarker maturity parameters: the role of generation and thermal degradation," *Organic Geochemistry*, vol. 29, no. 5-7, pp. 1181–1197, 1998.

[18] C. He, H. Huang, Q. Wang, and Z. Li, "Correlation of maturity parameters derived from Methylphenanthrenes and Methyldibenzothiophenes in the carboniferous source rocks from Qaidam Basin, NW China," *Geofluids*, vol. 2019, Article ID 5742902, 12 pages, 2019.

[19] J. M. Moldowan, P. Sundararaman, and M. Schoell, "Sensitivity of biomarker properties to depositional environment and/or source input in the Lower Toarcian of SW-Germany," *Organic Geochemistry*, vol. 10, no. 4-6, pp. 915–926, 1986.

[20] H. Zhang, H. Huang, Z. Li, and M. Liu, "Impact of maturation on the validity of paleoenvironmental indicators: implication for discrimination of oil genetic types in lacustrine shale systems," *Energy & Fuels*, vol. 34, no. 6, pp. 6962–6973, 2020.

[21] G. W. van Graas, "Biomarker maturity parameters for high maturities: Calibration of the working range up to the

oil/condensate threshold," *Organic Geochemistry*, vol. 16, no. 4-6, pp. 1025–1032, 1990.

[22] M. B. Allen, D. I. M. Macdonald, Z. Xun, S. J. Vincent, and C. Brouet-Menzies, "Early Cenozoic two-phase extension and late Cenozoic thermal subsidence and inversion of the Bohai Basin, northern China," *Marine and Petroleum Geology*, vol. 14, no. 7-8, pp. 951–972, 1997.

[23] B. Ma, Q. Hu, S. Yang et al., "Multiple approaches to quantifying the effective porosity of lacustrine shale oil reservoirs in Bohai Bay Basin, East China," *Geofluids*, vol. 2020, Article ID 8856620, 13 pages, 2020.

[24] S. Li, X. Pang, M. Li, and Z. Jin, "Geochemistry of petroleum systems in the Niuzhuang South Slope of Bohai Bay Basin–part 1: source rock characterization," *Organic Geochemistry*, vol. 34, no. 3, pp. 389–412, 2003.

[25] Z. Shen, B. Yu, C. Bai, S. Han, and H. Liu, "Origin of bedding-parallel calcite veins from lacustrine shale in the Eocene Dongying Depression, Bohai Bay Basin, China," *Geofluids*, vol. 2020, Article ID 8883297, 23 pages, 2020.

[26] Z. Zhan, X. Lin, Y. Zou et al., "Chemometric differentiation of crude oil families in the southern Dongying Depression, Bohai Bay Basin, China," *Organic Geochemistry*, vol. 127, pp. 37–49, 2019.

[27] X. Guo, S. He, K. Liu, G. Song, X. Wang, and Z. Shi, "Oil generation as the dominant overpressure mechanism in the Cenozoic Dongying depression, Bohai Bay basin, China," *AAPG Bulletin*, vol. 94, no. 12, pp. 1859–1881, 2010.

[28] X. Guo, K. Liu, S. He et al., "Petroleum generation and charge history of the northern Dongying depression, Bohai Bay basin, China: insight from integrated fluid inclusion analysis and basin modelling," *Marine and Petroleum Geology*, vol. 32, no. 1, pp. 21–35, 2012.

[29] H. Ping, H. Chen, and G. Jia, "Petroleum accumulation in the deeply buried reservoirs in the northern Dongying Depression, Bohai Bay Basin, China: new insights from fluid inclusions, natural gas geochemistry, and 1-D basin modeling," *Marine and Petroleum Geology*, vol. 80, pp. 70–93, 2017.

[30] H. Ping, H. Chen, S. C. George, C. Li, and S. Hu, "Relationship between the fluorescence colour of oil inclusions and thermal maturity in the Dongying Depression, Bohai Bay Basin, China: part 2. Fluorescence evolution of oil in the context of petroleum generation, expulsion and cracking under geological conditions," *Marine and Petroleum Geology*, vol. 103, pp. 306–319, 2019.

[31] P. Li, "Oil/gas distribution patterns in Dongying depression, Bohai Bay basin," *Journal of Petroleum Science and Engineering*, vol. 41, no. 1-3, pp. 57–66, 2004.

[32] C. Lampe, G. Song, L. Cong, and X. Mu, "Fault control on hydrocarbon migration and accumulation in the tertiary Dongying depression, Bohai Basin, China," *AAPG Bulletin*, vol. 96, no. 6, pp. 983–1000, 2012.

[33] D. Zhu, Z. Jin, W. Hu, Y. Song, and X. Gao, "Effect of igneous activity on hydrocarbon source rocks in Jiyang sub-basin, eastern China," *Journal of Petroleum Science and Engineering*, vol. 59, no. 3-4, pp. 309–320, 2007.

[34] L. Zhang, Q. Liu, R. Zhu, Z. Li, and X. Lu, "Source rocks in Mesozoic-Cenozoic continental rift basins, east China: a case from Dongying Depression, Bohai Bay Basin," *Organic Geochemistry*, vol. 40, no. 2, pp. 229–242, 2009.

[35] H. Zhang, H. Huang, Z. Li, and M. Liu, "Oil physical status in lacustrine shale reservoirs - a case study on Eocene Shahejie Formation shales, Dongying Depression, East China," *Fuel*, vol. 257, p. 116027, 2019.

[36] H. Zhang, H. Huang, Z. Li, and M. Liu, "Comparative study between sequential solvent-extraction and multiple isothermal stages pyrolysis: a case study on Eocene Shahejie Formation shales, Dongying Depression, East China," *Fuel*, vol. 263, article 116591, 2020.

[37] E. Lafargue, F. Marquis, and D. Pillot, "Rock–Eval 6 applications in hydrocarbon exploration, production, and soil contamination studies," *Revue de l'institut Français du Pétrole*, vol. 53, no. 4, pp. 421–437, 1998.

[38] B. P. Tissot, R. Pelet, and P. H. Ungerer, "Thermal history of sedimentary basins, maturation indices, and kinetics of oil and gas generation," *AAPG Bulletin*, vol. 71, pp. 1445–1466, 1987.

[39] X. Xie, M. Li, R. Littke et al., "Petrographic and geochemical characterization of microfacies in a lacustrine shale oil system in the Dongying Sag, Jiyang Depression, Bohai Bay Basin, eastern China," *International Journal of Coal Geology*, vol. 165, pp. 49–63, 2016.

[40] J. M. Moldowan, F. J. Fago, R. M. K. Carlson et al., "Rearranged hopanes in sediments and petroleum," *Geochimica et Cosmochimica Acta*, vol. 55, no. 11, pp. 3333–3353, 1991.

[41] M. Radke and D. H. Welte, "The methylphenanthrene index, MPI: a maturity parameter based on aromatic hydrocarbons," in *Advances in Organic Geochemistry 1981*, M. Bjoroy, Ed., pp. 504–512, Wiley, Chichester, UK, 1983.

[42] R. Alexander, R. I. Kagi, S. J. Rowland, P. N. Sheppard, and T. V. Chirila, "The effects of thermal maturity on distributions of dimethylnaphthalenes and trimethylnaphthalenes in some ancient sediments and petroleums," *Geochimica et Cosmochimica Acta*, vol. 49, no. 2, pp. 385–395, 1985.

[43] M. Radke, "Application of aromatic compounds as maturity indicators in source rocks and crude oils," *Marine and Petroleum Geology*, vol. 5, no. 3, pp. 224–236, 1988.

[44] M. Radke, D. H. Welte, and H. Willsch, "Geochemical study on a well in the Western Canada Basin: relation of the aromatic distribution pattern to maturity of organic matter," *Geochimica et Cosmochimica Acta*, vol. 46, no. 1, pp. 1–10, 1982.

[45] B. G. K. van Aarssen, T. P. Bastow, R. Alexander, and R. I. Kagi, "Distributions of methylated naphthalenes in crude oils: indicators of maturity, biodegradation and mixing," *Organic Geochemistry*, vol. 30, no. 10, pp. 1213–1227, 1999.

[46] M. Radke, D. H. Welte, and H. Willsch, "Maturity parameters based on aromatic hydrocarbons: Influence of the organic matter type," *Organic Geochemistry*, vol. 10, no. 1-3, pp. 51–63, 1986.

[47] A. S. Mackenzie, C. F. Hoffmann, and J. R. Maxwell, "Molecular parameters of maturation in the Toarcian shales, Paris Basin, France –III. Changes in aromatic steroid hydrocarbons," *Geochimica et Cosmochimica Acta*, vol. 45, no. 8, pp. 1345–1355, 1981.

[48] H. B. Lo, "Correction criteria for the suppression of vitrinite reflectance in hydrogen- rich kerogens: preliminary guidelines," *Organic Geochemistry*, vol. 20, no. 6, pp. 653–657, 1993.

[49] G. I. Unomah and C. M. Ekweozor, "Application of vitrinite reflectance in reconstruction of tectonic features in Anambra Basin, Nigeria: implication for petroleum potential," *AAPG Bulletin*, vol. 77, pp. 436–451, 1993.

[50] Y. Gong, L. Wang, and S. Liu, "Heat flow pattern of the Jiyang Depression," *Science in China Series D-Earth Sciences*, vol. 33, pp. 384–391, 2003.

[51] N. S. Qiu, X. G. Su, Z. Y. LI, Z. Q. Liu, and Z. Li, "The Cenozoic tectono-thermal evolution of Jiyang Depression, Bohai Bay Basin, East China," *Chinese Journal of Geophysics*, vol. 49, no. 4, pp. 1015–1024, 2006.

[52] Y. Zuo, N. Qiu, Y. Zhang et al., "Geothermal regime and hydrocarbon kitchen evolution of the offshore Bohai Bay basin, North China," *AAPG Bulletin*, vol. 95, no. 5, pp. 749–769, 2011.

[53] J. Teng, M. Mastalerz, B. Liu, T. Gognat, E. Hauser, and P. McLaughlin, "Variations of organic matter transformation in response to hydrothermal fluids: example from the Indiana part of the Illinois Basin," *International Journal of Coal Geology*, vol. 219, article 103410, 2020.

[54] C. Teng, F. Hao, H. Zou, X. Zhou, and C. Xu, "Tan–Lu fault system and its significance in oil accumulation in the central Liaodong Bay subbasin, Bohai Bay Basin, China," *AAPG Bulletin*, vol. 100, no. 2, pp. 289–314, 2016.